Acta Astronautica 95 (2014) 218–226

Contents lists available at ScienceDirect

Acta Astronautica

journal homepage: www.elsevier.com/locate/actaastro

High spin rate magnetic controller for nanosatellites ☆

A. Slavinskis [a,b,*], U. Kvell [a,b], E. Kulu [a,b], I. Sünter [a,b], H. Kuuste [a,b], S. Lätt [a,b], K. Voormansik [a,b], M. Noorma [a,b]

[a] Tartu Observatory, 61602 Tõravere, Tartu County, Estonia
[b] University of Tartu, Faculty of Science and Technology, Institute of Physics, Tähe 4-111, 51010 Tartu, Estonia

ARTICLE INFO

Article history:
Received 18 February 2013
Received in revised form
6 November 2013
Accepted 12 November 2013
Available online 20 November 2013

Keywords:
Magnetic attitude control
High spin rate control
Fault-tolerance
Hardware-in-the-loop
Nanosatellite
CubeSat

ABSTRACT

This paper presents a study of a high rate closed-loop spin controller that uses only electromagnetic coils as actuators. The controller is able to perform spin rate control and simultaneously align the spin axis with the Earth's inertial reference frame. It is implemented, optimised and simulated for a 1-unit CubeSat ESTCube-1 to fulfil its mission requirements: spin the satellite up to 360 deg s^{-1} around the z-axis and align its spin axis with the Earth's polar axis with a pointing error of less than 3°. The attitude of the satellite is determined using a magnetic field vector, a Sun vector and angular velocity. It is estimated using an Unscented Kalman Filter and controlled using three electromagnetic coils. The algorithm is tested in a simulation environment that includes models of space environment and environmental disturbances, sensor and actuator emulation, attitude estimation, and a model to simulate the time delay caused by on-board calculations. In addition to the normal operation mode, analyses of reduced satellite functionality are performed: significant errors of attitude estimation due to non-operational Sun sensors; and limited actuator functionality due to two non-operational coils. A hardware-in-the-loop test is also performed to verify on-board software.

1. Introduction

The development of nanosatellites has opened up new opportunities for space exploitation by decreasing average development times and mission costs [1]. Widespread use of the CubeSat standard [2] has enabled further reductions in average launch costs as standardised deployment systems have been developed for many different launchers. A wide range of general subsystems designed specifically for Cube Satellites is commercially available. Also, CubeSat developers often rely on the commercial off-the-shelf (COTS) components [3]. At the same time, strict limitations on mass and volume are challenging because of limited power production, limited computational performance as well as limited means of attitude measurements and control [4–6].

Despite these limitations, nanosatellites can accommodate more and more ambitious scientific payloads and technology for in-orbit demonstrations. Some experiments require active Attitude Determination and Control Systems (ADCS) using only electromagnetic actuation and on-board software of reduced computational complexity. [7–11].

Multiple nanosatellites have performed, or plan to perform, spin control using electromagnetic actuation. HAMSAT [12,13], Solar sail Cubesat [14], UOSAT [15] and TSUBAME [16] use B-dot [17] based spin controllers. Balaraman et al. [18] and Grahn [19] also discuss the B-dot based approach. FAST [20] and CINEMA [21] satellites use a two-stage controller (spin rate and precession) based on an analysis by Shigehara [22] and Grubin [23].

☆ This paper was presented during the 63rd IAC in Naples.

* Corresponding author. Tel.: +372 7376524.
E-mail addresses: andris.slavinskis@estcube.eu (A. Slavinskis), urmas.kvell@estcube.eu (U. Kvell), erik.kulu@estcube.eu (E. Kulu), indrek.sunter@estcube.eu (I. Sünter), henri.kuuste@estcube.eu (H. Kuuste), silver.latt@estcube.eu (S. Lätt), kaupo.voormansik@estcube.eu (K. Voormansik), mart.noorma@estcube.eu (M. Noorma).

0094-5765/$ - see front matter © 2013 IAA. Published by Elsevier Ltd. All rights reserved.
http://dx.doi.org/10.1016/j.actaastro.2013.11.014

Ovchinnikov et al. [24] have developed a controller that can also be implemented as a two-stage controller. The magnetic fault-tolerant spin stabilising controller for the JC2Sat-FF mission [25] stands out with its efficient simultaneous control of spin rate and alignment of the spin axis with the Earth's inertial reference frame. However, the use of this controller for high spin rate control (magnitudes of hundreds of deg s^{-1}) has not previously been examined.

This study presents a spin control algorithm, which has been implemented, optimised and simulated for a 1-unit CubeSat [2] ESTCube-1 [26,27]. Monte Carlo simulation results of a fully operational satellite are presented. Two analyses of the satellite of reduced functionality are carried out, in the first instance by simulating non-operational Sun sensors and in the second instance by simulating two non-operational coils. Hardware-in-the-loop (HIL) test results are presented.

The spin control algorithm is implemented and tested in a MATLAB® Simulink® space simulation environment [28,29] that includes models of space environment and environmental disturbance, sensor and actuator emulation, an Unscented Kalman Filter (UKF) [30] for attitude estimation, and a model to simulate the time delay caused by on-board calculations.

2. Requirements

While there could be many applications of magnetic satellite spin control for nanosatellites (e.g., spin-stabilisation), this paper studies the use of controller for the ESTCube-1 satellite to fulfil the following mission requirement: spin the satellite up to 360 deg s^{-1} around the z-axis (major axis of inertia) and align its spin axis with the Earth's polar axis with a pointing error of less than 3°. This mission is the first in-space Electric Solar Wind Sail (E-sail) [31] experiment carried out on the ESTCube-1 satellite, a 1-unit, 1.1 kg CubeSat that will be in Sun-synchronous polar orbit at an altitude of $\approx$680 km. The satellite will use the centrifugal force provided by spin-up manoeuvre to deploy a 10 m long tether. A rather high value of angular rate of 360 deg s^{-1} was selected to ensure a high enough tether tension to pull the tether out from the reel reliably. The angular rate of 360 deg s^{-1} will decrease to $\approx$20 deg s^{-1} during tether deployment due to angular momentum conservation. After tether deployment, the E-sail experiment will be run by charging the tether synchronously with the satellite spin to increase and decrease the satellite angular rate by employing the Coulomb drag force. In a polar orbit, the Coulomb drag force changes the spin rate of the tether maximally when the orbital velocity vector lies in the spin plane. Tilting of the spin plane caused by the magnetic Lorentz force should be avoided. Having the spin plane aligned with the equatorial plane and running the experiment near the Earth's geographical poles provides a set-up with a maximal influence of the Coulomb drag force and a minimal spin plane tilt caused by the magnetic Lorentz force because the magnetic field is perpendicular to the spin plane. An alignment error of less than 3° is a safe selection for the influence of the Coulomb drag force to be big enough and of the magnetic Lorentz force to be small enough. The ESTCube-1 ground station is located at an approximate latitude of 58° North. ESTCube-1 has monopole antennas perpendicular to the z-axis. This set-up provides a communication link without blind spots even if the satellite has a high spin rate around the satellite z-axis that is aligned with the Earth's polar axis. [27]

The attitude determination system uses three-axis magnetometers, three-axis gyroscopic sensors and two-axis Sun sensors, one on each side of the satellite. Attitude estimation is performed using an UKF and attitude control is performed by three electromagnetic coils.

The electrical power system is able to provide constantly 150 mW from batteries for coils for more than 30 orbits in the worst-case scenario assuming that no power is generated by solar panels. Since each side of the satellite is covered with two solar panels, power generation of a spinning satellite should not drop below the estimated worst-case scenario of 2.2 W assuming that one side of the satellite is directed towards the Sun. [26]

To mitigate the risk of mission failure due to hardware malfunction, analyses of reduced satellite functionality are carried out. While magnetometer and gyroscope failure would lead to failure of the mission, this risk is mitigated by the use of two magnetometers and four gyroscopes. Sun sensor failure would increase errors in estimated attitude. Worst-case scenario analysis is carried out by simulating spin control when all Sun sensors fail. The implications of failed magnetic actuators are described by de Ruiter [25]. Analysis shows that the spin controller is able to reach the desired state even when up to two coils fail, providing that the working coil is perpendicular to the spin plane. In this paper, this worst-case scenario analysis is carried out by simulating spin control when two coils fail (x–z and y–z).

To mitigate the risk of software failure, a HIL test is carried out on a MCU prototype with the same processor and memory capacity as on the flight hardware.

3. Space simulation environment

The space simulation environment is a set of adjustable and expandable models and signal processing tools that interact with each other to provide a realistic basis for modelling attitude determination and control.

In this analysis, the following reference frames are used. First, the Earth Centred Inertial reference Frame (ECIF): the origin of the frame is at the centre of the Earth, the x-axis passes through the point where the vernal equinox and equatorial plane intersect, and the z-axis passes through the Geographic North Pole. Second, the Earth Centred Earth Fixed reference frame (ECEF): the origin of the frame is at the centre of the Earth, the x-axis passes through the point where the Greenwich Meridian intersects the equatorial plane, and the z-axis passes through the Geographic North Pole. Third, the Satellite Body Reference Frame (SBRF): the origin of the frame is at the geometrical centre of the satellite and all axes are aligned with the satellite frame. According to Vinther et al. [30], the rotation between the SBRF and the principal reference frame is not required since 1-unit CubeSats are close to symmetric in terms of mass distribution.

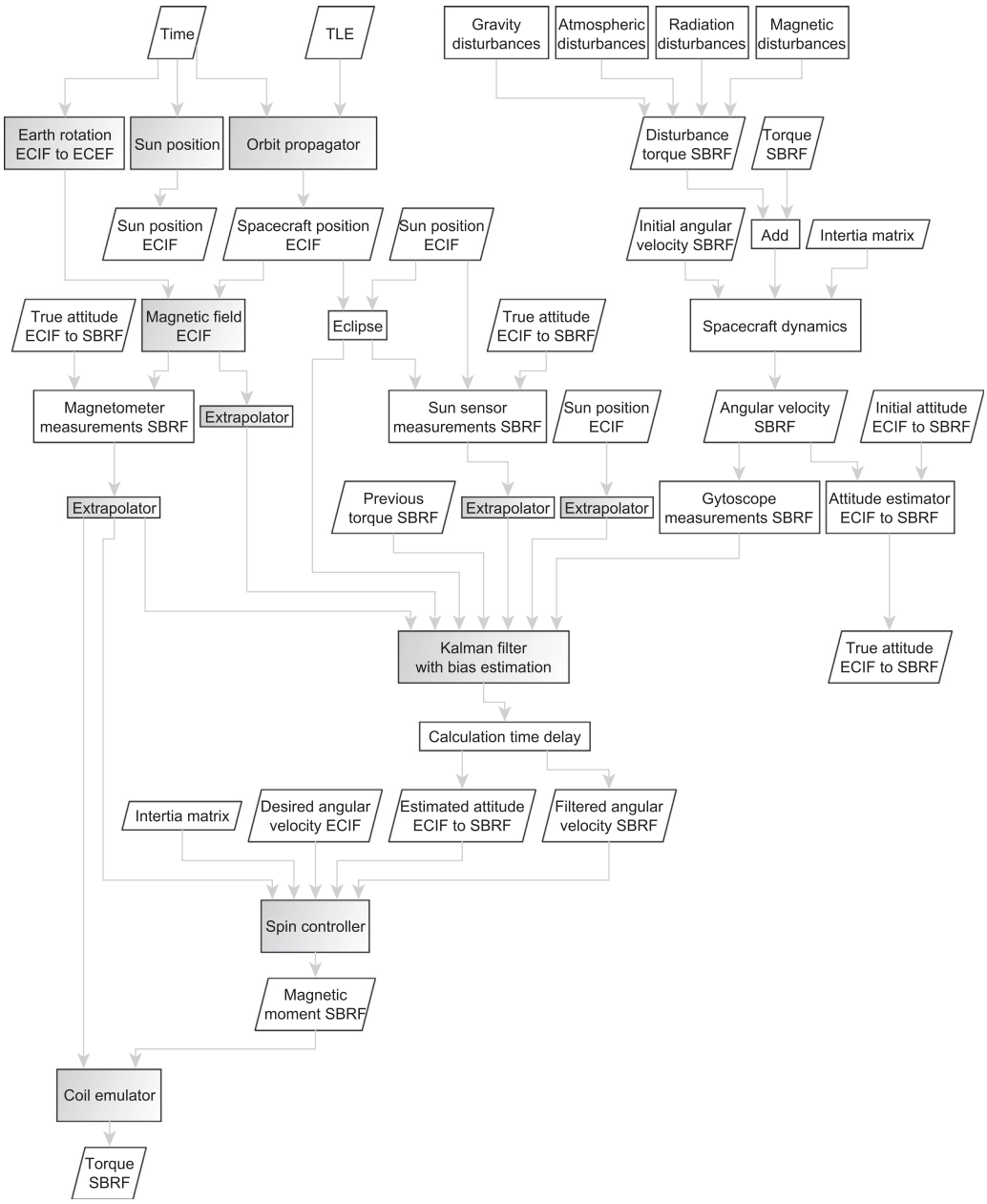

Fig. 1. Space simulation environment schematic. Blocks marked with a grey background are also implemented on-board.

The schematic of the simulation environment is presented in Fig. 1. The Sun's position is calculated using the algorithm presented in [32, p. 36]. The orbit is propagated using the Simplified General Perturbations Model 4 [33]. Magnetic field is calculated using International Geomagnetic Reference Field 11 [34]. The Earth's rotation model, the eclipse model and models of disturbances are described by Amini et al. [28], Jensen and Vinther [29]. Satellite dynamics and kinematics are based on derivations described by Wertz [35, p. 510–524]. Sensor measurements are modelled by transforming the corresponding vector to the SBRF and applying Gaussian noise with a given standard deviation. The UKF is used for estimating attitude [30]. The UKF also performs bias estimation for all sensor data. The spin controller is described in detail in Section 4.

One iteration of on-board calculations can take up to 0.2 s; when approaching the desired spin rate of 360 deg s^{-1}, the attitude can change by up to 72° while these calculations are being performed. In the simulation environment, this is modelled as a calculation time delay. Because the calculation time delay can cause significant error in the estimated attitude, results from models and sensor readings are extrapolated before being passed to the UKF. Spacecraft position, Sun position and Earth rotation are extrapolated by passing the sum of the current time and the time estimated for calculations to the

respective model. The extrapolated spacecraft position passed to the magnetic field model provides an extrapolated magnetic field vector. Angular velocity is constant during calculation because no control torque is applied and disturbance torques can be considered negligible. The angular velocity and the estimated calculation time provide the change of attitude used to extrapolate magnetometer and Sun sensor measurements.

The coil emulator saturates and quantises the magnetic moment to calculate torque. Saturation is caused by maximum coil current. Each element of the magnetic moment vector is quantised to a signed 9-bit value to comply with on-board implementation.

Because of the high spin rate, special attention should be paid to the frequency and duration of the applied torque. Taking coil discharge time, measurement time, calculation time and torque time into account, it was found that the whole cycle can be run with an attitude determination and control frequency of 3 Hz. One complete cycle is shown in Fig. 2. Tests showed coil discharge time to be less than 0.02 s, measurement time less than 0.013 s and calculation time less than 0.17 s (given with the safety margin in Fig. 2). Simulations of different torque times showed best spin-up performance when the torque time was set to 0.1 s.

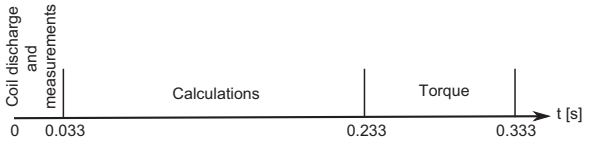

Fig. 2. Timeline of one attitude determination and control cycle.

The schematic of HIL set-up is presented in Fig. 3. Sensor readings are emulated in the simulation environment and together with the eclipse parameter and time are sent to the MCU. A serial port with an USB (Universal Serial Bus)-to-serial converter is used for communication. On the MCU, the Earth rotation model, the Sun position model, orbit propagation and the magnetic field model are run. Based on models, emulated sensor readings, eclipse parameter and time, the UKF estimates attitude as an input to the spin controller. Then magnetic moment values from the spin controller are quantised, saturated and sent to the simulation environment. In orbit, the eclipse parameter will be derived from Sun sensor and solar panel readings. It also indicates whether the Sun is in the field of view.

Simulation environment parameters are listed in Table 1.

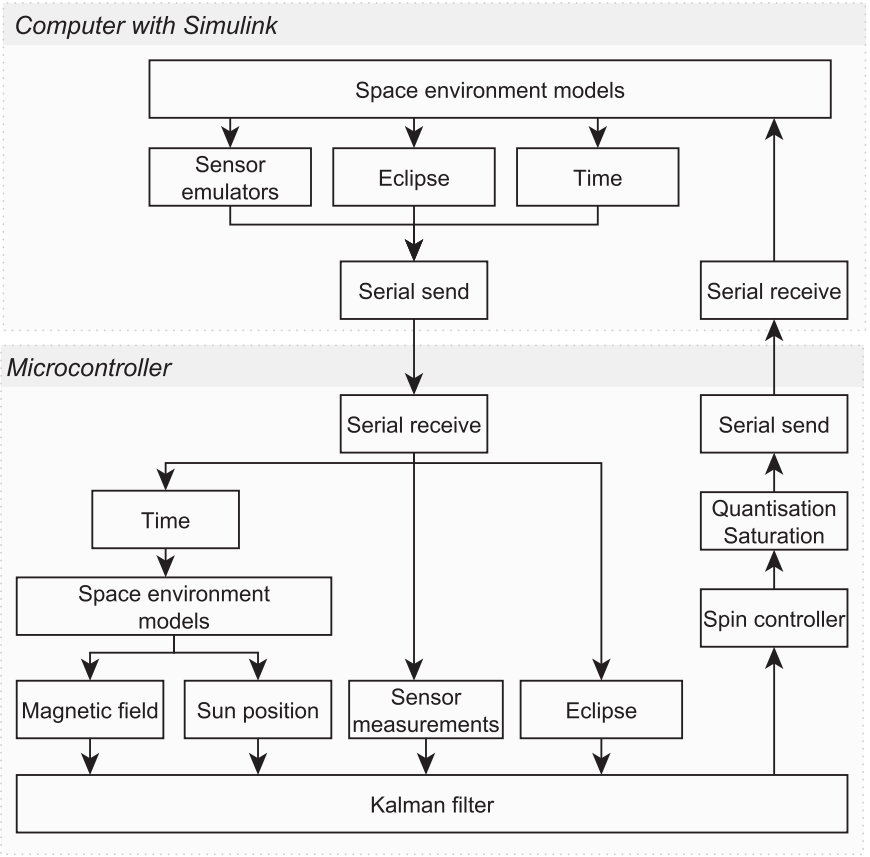

Fig. 3. Hardware-in-the-loop schematic.

4. Spin controller

The spin controller, based on Lyapunov approach, simultaneously performs spin rate control and spin axis alignment. It is described with Formulae (1)–(4) [25]. The first term in parentheses of Formula (2) controls the spin rate; the second term minimises the effect of precession and the third is a nutation dumping term. In the presence of errors it is required for the dipole moment $\boldsymbol{m}$ to have a correct sign for the controller to be stable. The controller's stability requirement sets a complex requirement for the angular velocity measurement accuracy, the magnetic field measurement accuracy, the overall attitude estimation accuracy and the moment of inertia determination accuracy since the dipole moment is a function of all listed parameters. In order for the rotation to be stable, the satellite should spin around the minor or major axis of inertia. In order for the controller to reach the desired state, control gains should be set as follows: $k>0$, $k_1>1$ and $k_2>0$. It is suggested to select k such that it does not saturate the control signal; k_1 between 1 and 2; and k_2 to be small. During development of the spin controller, two reasonable assumptions have been made. First, the local Earth's magnetic field vector expressed in an inertial frame is a uniformly continuous function of time and its absolute value is bounded by two positive values. Second, it is impossible for the satellite's natural motion to match the time history of the Earth's magnetic field throughout the orbit. The satellite spin axis might end up pointing the opposite direction to what is expected but such behaviour has not been observed by both the author of the spin controller and authors of this paper. The spin controller is able to reach the desired state in the case of two out of three failed coils, providing that the working coil is perpendicular to the spin plane. If the only working coil is parallel to the spin plane, the spin controller is not able to reach the desired state. [25]

$$\boldsymbol{m}=sat\left[-\frac{k}{\|\boldsymbol{B}\|^2}\boldsymbol{A},m_{max}\right] \tag{1}$$

$$\boldsymbol{A}=\boldsymbol{WB}\times\left(\tilde{\boldsymbol{h}}+k_1 e_{hz}\begin{bmatrix}0\\0\\1\end{bmatrix}+k_2\boldsymbol{P\omega}\right) \tag{2}$$

$$\tilde{\boldsymbol{h}}=\boldsymbol{h}-\boldsymbol{h}_d=\boldsymbol{I\omega}-\boldsymbol{I\omega}_d \tag{3}$$

$$e_{hz}=h_z-h_{d\omega}=I_z\omega_z-I_z\omega_{d\omega} \tag{4}$$

$\boldsymbol{m}$ is the magnetorquer dipole moment vector expressed in the SBRF.
$\boldsymbol{B}$ is the is Earth's magnetic field vector expressed in the SBRF.
$\boldsymbol{h}$ is the satellite angular momentum vector expressed in the SBRF; $\boldsymbol{h}=[h_x\ h_y\ h_z]^T$.
$\boldsymbol{h}_d$ is the desired satellite angular momentum vector expressed in the SBRF; $\boldsymbol{h_d}=[h_{dx}\ h_{dy}\ h_{dz}]^T$.
$\tilde{\boldsymbol{h}}$ is the satellite angular momentum error vector expressed in the SBRF.
$\boldsymbol{I}$ is the satellite moment of inertia matrix expressed in the SBRF; $\boldsymbol{I}=diag(I_x,I_y,I_z)$.
$\boldsymbol{\omega}$ is the satellite angular velocity vector expressed in the SBRF; $\boldsymbol{\omega}=[\omega_x\ \omega_y\ \omega_z]^T$.
$\boldsymbol{\omega}_d$ is the desired satellite angular velocity vector defined in the ECIF and expressed in the SBRF;

Table 1
Space simulation environment parameters.

Parameter name	Value
Satellite mass	1.12513 kg
Satellite size	$0.1\times0.1\times0.11$ m
Centre of mass	$[0.04847\ 0.04797\ 0.04928]^T$ m
Inertia matrix	diag [0.0020849 0.002259 0.0022989] kg m^2
Atmospheric drag coefficient	2.0
Atmospheric density	10^{-13} kg m^{-3}
Solar momentum flux	4.5565 N m^{-2}
Solar absorption coefficient	1.2964
Maximum magnetic moment for coils	0.104 A m^2
Magnetometer standard deviation	3°
Sun sensor standard deviation	3.33°
Gyroscope standard deviation	1 deg s^{-1}
Attitude determination and control frequency	3 Hz
Calculation time	0.2 s
Torque time	0.1 s
Coil discharge and measurement time	0.033 s
TLE epoch	13859.424
TLE BSTAR drag term	0.14573×10^3(Earth radii)$^{-1}$
TLE inclination	98°
TLE right ascension of ascending node	161°
TLE eccentricity	0.0015763
TLE argument of perigee	22°
TLE mean anomaly	338°
TLE mean motion	14.66309673 rev day^{-1}

$\boldsymbol{\omega}_d = [\omega_{dx}\ \omega_{dy}\ \omega_{dz}]^T$.
e_{hz} is the angular momentum error around the satellite's z-axis.
$h_{d\omega}$ is the desired angular momentum around the satellite's z-axis.
$\omega_{d\omega}$ is the desired angular speed defined and expressed in the SBRF.
k is the controller gain for overall convergence.
k_1 is the controller gain for precession damping.
k_2 is the controller gain for nutation damping.
$\boldsymbol{P}$ is the x- and y-axis selection matrix; $\boldsymbol{P} = diag(1, 1, 0)$.
$\boldsymbol{W}$ is the coil selection matrix; if all coils are active, $\boldsymbol{W} = diag(1, 1, 1)$.

The saturation function of the ith element is defined by Formula (5).

$$\{sat[\boldsymbol{x}, \boldsymbol{x}_{max}]\}_i = \begin{cases} \{\boldsymbol{x}\}_i, & |\{\boldsymbol{x}\}_i| \le \{\boldsymbol{x}_{max}\}_i \\ \{\boldsymbol{x}_{max}\}_i sign(\{\boldsymbol{x}\}_i) & |\{\boldsymbol{x}\}_i| > \{\boldsymbol{x}_{max}\}_i \end{cases} \quad (5)$$

5. Simulation results

Spin controller simulation results are presented in this section. Simulations of a fully operational satellite show controller performance with all coils and sensors working. Two types of fault-tolerance simulation are presented: first, with significant errors in estimated attitude caused by non-operational Sun sensors and, second, with two non-operational coils. A HIL test is performed to test the on-board software.

The desired angular velocity vector is given in the ECIF as $\boldsymbol{\omega}_d = [0\ 0\ 360]^T$ deg s^{-1} and in each iteration it is transformed to the SBRF by using an attitude quaternion. The desired angular velocity is directly defined in the SBRF as $\omega_{d\omega} = 360$ deg s^{-1}. Effective gain values k, k_1, k_2 were found iteratively to be 0.001, 1.3, 0.1, respectively.

Initial angular velocities were set randomly between -2 deg s^{-1} and $+2$ deg s^{-1} around all axes. The initial conditions can be achieved by using a B-dot [17] detumbling controller that can detumble the satellite from angular velocities of magnitude of up to 200 deg s^{-1} down to as low as 0.2 deg s^{-1}.

The desired state is defined as follows: angular velocity around the SBRF z-axis should be ≈ 360 deg s^{-1} and the pointing error between the SBRF and the ECIF z-axes should be less than 3°. There are no strict requirements for the maximum permissible spin rate control error because the experiment does not depend on an exact control of spin rate but rather on precise measurements of the spin rate.

5.1. Fully operational satellite

During all simulations, the fully operational satellite reached the desired state within a maximum of three orbits. Results are presented in Fig. 4. Fig. 4a shows results of the simulation that took the most time to reach the desired state. Left y-axis shows the satellite angular velocity expressed in the ECIF. Right y-axis shows the satellite pointing error between the SBRF and the ECIF z-axes. Fig. 4b shows results after the third orbit for all simulations. Left y-axis shows the satellite angular velocity around the z-axis expressed in the ECIF. Right y-axis shows the pointing error between the SBRF and the ECIF z-axes as well as the 3° limit of the maximum permissible satellite pointing error. During first two orbits, when coils are used actively, average power consumption of all coils summed is less than 130 mW.

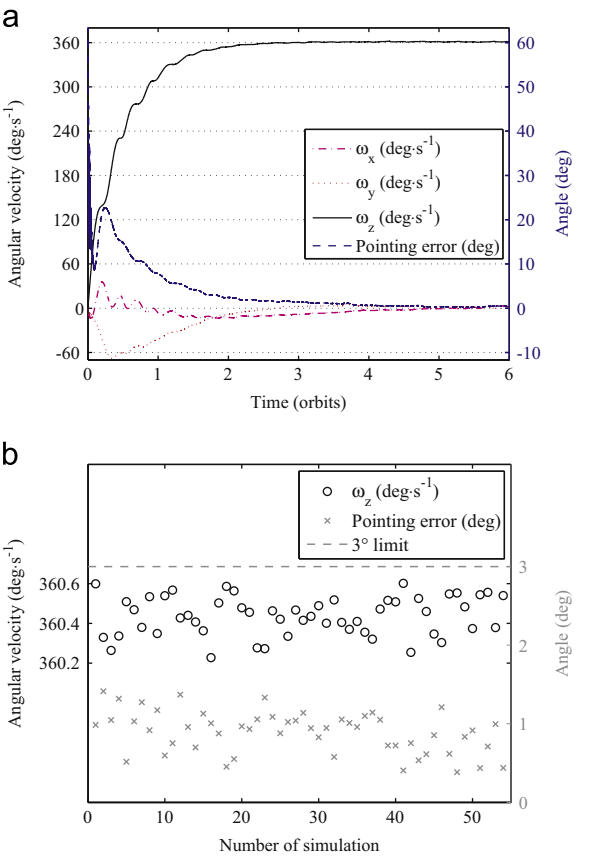

Fig. 4. Fully operational satellite. (a) Results of the simulation that took the most time to reach the desired state. Left y-axis: satellite angular velocity expressed in the ECIF. Right y-axis: satellite pointing error between the SBRF and the ECIF z-axes. (b) Results after the third orbit for all simulations. Left y-axis: satellite angular velocity around the z-axis expressed in the SBRF. Right y-axis: pointing error between the SBRF and the ECIF z-axes.

5.2. Non-operational Sun sensors

During all simulations with non-operational Sun sensors, the satellite reached the desired state within a maximum of 10 orbits. Fig. 5a shows results of the simulation that took the most time to reach the desired state. Fig. 5b shows results after orbit number 10 for all simulations. During first eight orbits, when coils are used actively, average power consumption of all coils summed is less than 120 mW.

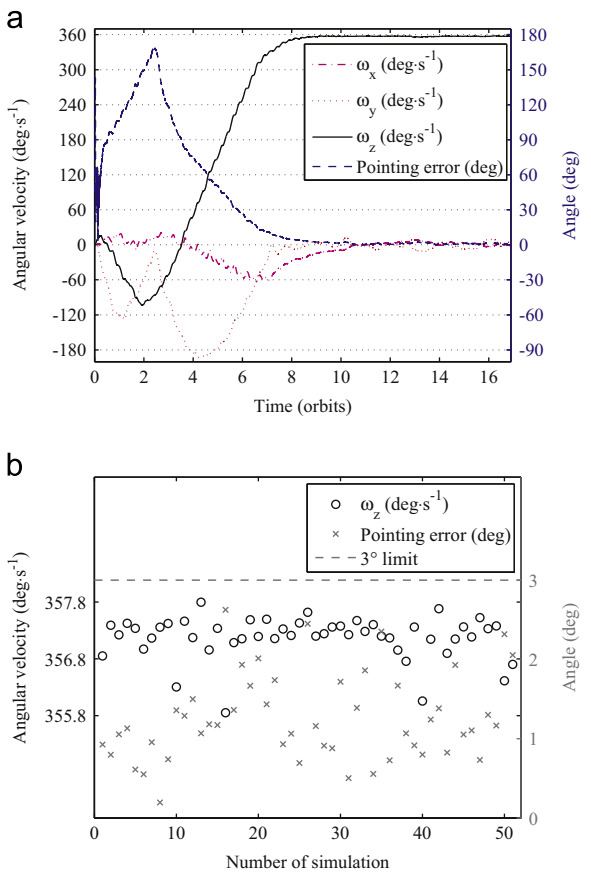

Fig. 5. Non-operational Sun sensors. (a) Results of the simulation that took the most time to reach the desired state. Left *y*-axis: satellite angular velocity expressed in the ECIF. Right *y*-axis: satellite pointing error between the SBRF and the ECIF *z*-axes. (b) Results after orbit number 10 for all simulations. Left *y*-axis: satellite angular velocity around the *z*-axis expressed in the SBRF. Right *y*-axis: pointing error between the SBRF and the ECIF *z*-axes.

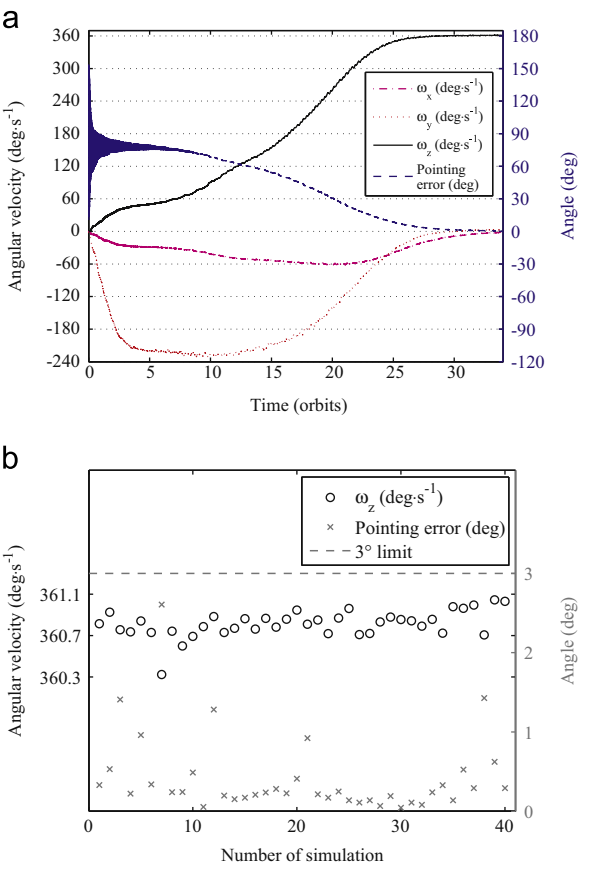

Fig. 6. Two non-operational coils. (a) Results of the simulation that took the most time to reach the desired state. Left *y*-axis: satellite angular velocity expressed in the ECIF. Right *y*-axis: satellite pointing error between the SBRF and the ECIF *z*-axes. (b) Results after orbit number 30 for all simulations. Left *y*-axis: satellite angular velocity around the *z*-axis expressed in the SBRF. Right *y*-axis: pointing error between the SBRF and the ECIF *z*-axes.

5.3. Two non-operational coils

During all simulations with non-operational *x*–*z* or *y*–*z* coils, the satellite reached the desired state within a maximum of 30 orbits. Fig. 6a shows results of the simulation that took the most time to reach the desired state. Fig. 6b shows results after orbit number 30 for all simulations. During first 25 orbits, when coils are used actively, average power consumption of all coils summed is less than 40 mW.

5.4. Hardware-in-the-loop

The HIL test was run on a MCU with the STM32F103 processor. The processor's clock frequency was set to 72 MHz. A single iteration of ADCS software takes ≈ 160 ms when executed together with command and data management tasks. RAM (Random-Access Memory) footprint is ≈ 4.5 kB and flash memory footprint ≈ 54 kB. The satellite was fully operational in this simulation.

Results are presented in Fig. 7. The satellite reached the desired state within five orbits. The performance is not as efficient as in Section 5.1 due to high-speed communication problems between the MCU and Simulink. The simulation environment missed a part of data due to the fact that only simulation step size is controllable but not the data rate of serial communication. However, ability to perform in the presence of errors has showed fault-tolerance of the spin controller. During first four orbits, when coils are used actively, average power consumption of all coils summed is less than 125 mW.

6. Conclusions

This analysis demonstrates that it is possible to perform high rate spin control and simultaneous spin axis alignment with the Earth's inertial reference frame for a nanosatellite, using only electromagnetic coils as actuators. The requirements of the desired state are that the angular velocity around the SBRF *z*-axis should reach ≈ 360 deg s^{-1}, and that the pointing error between the SBRF and the ECIF *z*-axes should be less than 3°. Simulations of a fully operational satellite demonstrated that the desired state could be attained within three orbits.

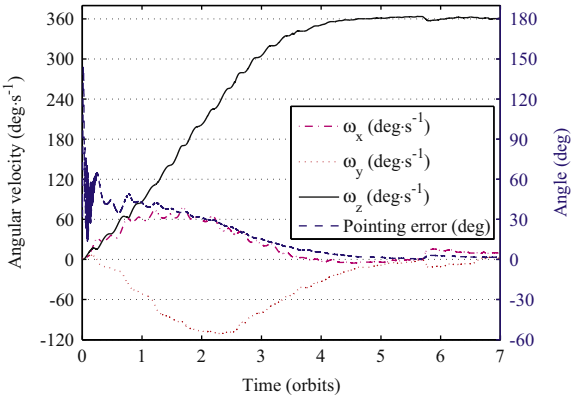

Fig. 7. Hardware-in-the-loop simulation. Left *y*-axis: satellite angular velocity expressed in the ECIF. Right *y*-axis: pointing error between the SBRF and the ECIF *z*-axes.

Controller fault-tolerance was analysed. When significant errors of estimated attitude were caused by non-operational Sun sensors, the desired state was reached within 10 orbits; with two non-operational coils it was reached within 30 orbits; and in the presence of communication errors during the HIL test the desired state was reached within five orbits. Even in the worst-case, the fault-tolerance test demonstrates the ability to reach the desired state in ≈ 2 days. All simulations showed power consumption for coils within required limit. These results are sufficient to satisfy the ESTCube-1 and E-sail mission requirements.

The HIL test showed that it is possible to run the software of an active ADCS on the hardware of a nanosatellite, i.e., STM32F103 processor, at least 4.5 kB of RAM and 54 kB of flash memory. In order to increase performance it is suggested to use a hardware floating-point unit for 64-bit floating point arithmetic.

Acknowledgements

The authors would like to thank everybody who is working and has worked on ESTCube-1; especially those involved in the ADCS and Mihkel Pajusalu. Pekka Janhunen (Finnish Meteorological Institute) is greatly acknowledged for his contribution to the ESTCube-1 mission. We also thank the AAUSAT team (Aalborg University, Denmark) for providing the space simulation environment and Jesper A. Larsen for answering many questions about attitude determination and control.

This research was supported by European Social Fund's Doctoral Studies and Internationalisation Programme DoRa.

References

[1] J. Bouwmeester, J. Guo, Survey of worldwide pico- and nanosatellite missions, distributions and subsystem technology, Acta Astronaut. 67 (2010) 854–862, http://dx.doi.org/10.1016/j.actaastro.2010.06.004.

[2] The CubeSat Program, Cal Poly SLO, CubeSat Design Specification Rev. 12 (2009). URL: ⟨http://www.cubesat.org/images/developers/cds_rev12.pdf⟩.

[3] K. Woellert, P. Ehrenfreund, A.J. Ricco, H. Hertzfeld, Cubesats: cost-effective science and technology platforms for emerging and developing nations, Adv. Space Res. 47 (2011) 663–684, http://dx.doi.org/10.1016/j.asr.2010.10.009.

[4] M. Pajusalu, E. Ilbis, J. Kalde, H. Lillmaa, R. Reinumägi, R. Rantsus, M. Pelakauskas, A. Leitu, V. Allik, M. Noorma, S. Lätt, J. Envall, Electrical power system for ESTCube-1: a fault-tolerant COTS solution, in: 63rd International Astronautical Congress, 2012, ISSN: 1995-6258.

[5] S.D. Jong, G. Aalbers, J. Bouwmeester, Improved command and data handling system for the Delfi-n3Xt nanosatellite, in: 59th International Astronautical Congress, vol. 4, 2008, pp. 2428–2441, ISBN: 9781615671601.

[6] A. Addaim, A. Kherras, E.B. Zantou, Aerospace Technologies Advancements, InTech, 2010, pp. 293–318, http://dx.doi.org/10.5772/6925.

[7] D. Selva, D. Krejci, A survey and assessment of the capabilities of Cubesats for Earth observation, Acta Astronaut. 74 (2012) 50–68, http://dx.doi.org/10.1016/j.actaastro.2011.12.014.

[8] M. Ansdell, P. Ehrenfreund, C. McKay, Stepping stones toward global space exploration, Acta Astronaut. 68 (2011) 2098–2113, http://dx.doi.org/10.1016/j.actaastro.2010.10.025.

[9] P. Ehrenfreund, C. McKay, B.H. Foing, JohnD. Rummel, C.R. Neal, T. Masson-Zwaan, M. Ansdell, N. Peter, J. Zarnecki, S. Mackwell, M. A. Perino, L. Billings, J. Mankins, M. Race, Toward a global space exploration program: a stepping stone approach, Adv. Space Res. 49 (2012) 2–48, http://dx.doi.org/10.1016/j.asr.2011.09.014.

[10] P. Weiss, W. Leung, K. Yung, Feasibility study for near-earth-object tracking by a piggybacked micro-satellite with penetrators, Planet. Space Sci. 56 (2010) 913–919.

[11] J.C. Springmann, A.J. Sloboda, A.T. Klesh, M.W. Bennett, J.W. Cutler, The attitude determination system of the RAX satellite, Acta Astronaut. 75 (2012) 120–135, http://dx.doi.org/10.1016/j.actaastro.2012.02.001.

[12] P. Natarajan, P. Pandey, V. Agrawal, N. Malik, Autonomous spin axis and spin rate control of HAMSAT, in: 58th International Astronautical Congress, vol. 6, 2007, pp. 3595–3600, ISBN: 978-1-60560-150-2.

[13] N.V. Vighnesam, A. Sonney, P.K. Soni, HAMSAT-1 precise orbit determination system and performance, J. Spacecr. Rockets 44 (2007) 727–731, http://dx.doi.org/10.2514/1.28876.

[14] W.H. Steyn, V. Lappas, Cubesat solar sail 3-axis stabilization using panel translation and magnetic torquing, Aerosp. Sci. Technol. 15 (2011) 476–485, http://dx.doi.org/10.1016/j.ast.2010.09.009.

[15] M.S. Hodgart, Attitude control and dynamics of UOSAT angular motion, Radio Electron. Eng. 52 (1982) 379–384, http://dx.doi.org/10.1049/ree.1982.0055.

[16] J. Nishida, Y. Tsubuku, Tokyo Tech's technology demonstration satellite TSUBAME, in: 21st AAIA/USC Conference on Small Satellites, vol. 21, 2007.

[17] T.W. Flatley, W. Morgenstern, A. Reth, F. Bauer, A B-dot acquisition controller for the RADARSAT spacecraft, in: Flight Mechanics Symposium, Stanford, CA, 1997, pp. 79–89, ark:/13960/t01z52w04.

[18] S. Balaraman, J. Shanmugam, P. Natarajan, S. Thambiurai, Magnetic attitude control for a spinning spacecraft with cross product of inertia, in: IEEE Aerospace Conference, 2009, pp. 1–7, http://dx.doi.org/10.1109/AERO.2009.4839584.

[19] S. Grahn, An on-board algorithm for automatic sun-pointing of a spinning satellite, Technical Report, Science Systems Division, Swedish Space Corporation, 2011, URL: ⟨http://www.svengrahn.pp.se/histind/astrid2/solpoint.pdf⟩.

[20] R.F. Pfaff (Ed.), The Fast Mission, Kluwer Academic Publishers, 2001. ISBN: 978-0-7923-7046-8.

[21] K.P. Vega, D. Auslander, D. Pankow, Design and modeling of an active attitude control system for CubeSat class satellites, in: AIAA Modeling and Simulation Technologies Conference, 2009, http://dx.doi.org/10.2514/6.2009-5812.

[22] M. Shigehara, Geomagnetic attitude control of an axisymmetric spinning satellite, J. Spacecr. Rockets 9 (1972) 391–398, http://dx.doi.org/10.2514/3.61700.

[23] C. Grubin, Satellite attitude determination by simultaneous line-of-sight sightings, J. Spacecr. Rockets 14 (1977) 640, http://dx.doi.org/10.2514/3.57245.

[24] M. Ovchinnikov, D. Roldugin, V. Penkov, Asymptotic study of a complete magnetic attitude control cycle providing a single-axis orientation, Acta Astronaut. 77 (2012) 48–60, http://dx.doi.org/10.1016/j.actaastro.2012.03.001.

[25] A. de Ruiter, A fault-tolerant magnetic spin stabilizing controller for the JC2Sat-FF mission, Acta Astronaut. 68 (2011) 160–171, http://dx.doi.org/10.1016/j.actaastro.2010.07.012.

[26] M. Pajusalu, R. Rantsus, M. Pelakauskas, A. Leitu, E. Ilbis, J. Kalde, H. Lillmaa, R. Reinumägi, K. Voormansik, K. Zālīte, V. Allik, M. Noorma, S. Lätt, Design of the electrical power system for the ESTCube-1 satellite, Latv. J. Phys. Tech. Sci. 49 (2012) 16–24, http://dx.doi.org/10.2478/v10047-012-0014-4.
[27] P. Janhunen, P.K. Toivanen, J. Polkko, S. Merikallio, P. Salminen, E. Hæggström, H. Seppänen, R. Kurppa, J. Ukkonen, S. Kiprich, G. Thornell, H. Kratz, L. Richter, O. Krömer, R. Rosta, M. Noorma, J. Envall, S. Lätt, G. Mengali, A.A. Quarta, H. Koivisto, O. Tarvainen, T.Kalvas, J. Kauppinen, A. Nuottajärvi, A. Obraztsov, Electric solar wind sail: toward test missions, Rev. Sci. Instrum 81 (2010) 111301:1–11, http://dx.doi.org/10.1063/1.3514548.
[28] R. Amini, J.A. Larsen, R. Izadi-Zamanabadi, D.D.V. Bhanderi, Design and implementation of a space environment simulation toolbox for small satellites, in: 56th International Astronautical Congress, vol. 9, 2005, pp. 6207–6213, ISBN: 978-1-60423-648-4.
[29] K.F. Jensen, K. Vinther, Attitude Determination and control system for AAUSAT3, Master's Thesis, Aalborg University, 2010.
[30] K. Vinther, K.F. Jensen, J.A. Larsen, R. Wiśniewski, Inexpensive CubeSat attitude estimation using quaternions and unscented Kalman filtering, Online J. Autom. Control Aerosp. (2011), ISSN: 1974-5168, URL: ⟨http://www.aerospace.unibo.it/?a=abstract&id=64⟩.
[31] P. Janhunen, Electric sail for spacecraft propulsion, J. Propul. Power 20 (2004) 763–764, http://dx.doi.org/10.2514/1.8580.
[32] O. Montenbruck, T. Pfleger, Astronomy on the Personal Computer, Springer Verlag, 1991 ISBN: 978-3-540-67221-0.
[33] F.R. Hoots, R.L. Roehrich, Spacetrack Report No. 3—Models for Propagation of NORAD Element Sets, Technical Report, Peterson AFB: Office of Astrodynamics, Aerospace Defense Center, 1980, URL ⟨http://www.celestrak.com/NORAD/documentation/spacetrk.pdf⟩.
[34] C.C. Finlay, S. Maus, C.D. Beggan, T.N. Bondar, A. Chambodut, T. A. Chernova, A. Chulliat, V.P. Golovkov, B. Hamilton, M. Hamoudi, R. Holme, G. Hulot, W. Kuang, B. Langlais, V. Lesur, F.J. Lowes, H. Luhr, S. Macmillan, M. Mandea, S. McLean, C. Manoj, M. Menvielle, I. Michaelis, N. Olsen, J. Rauberg, M. Rother, T. J. Sabaka, A. Tangborn, L. Toffner-Clausen, E. Thebault, A.W. P. Thomson, I.W.Z. Wei, T.I. Zvereva, International geomagnetic reference field: the eleventh generation, Geophys. J. Int. 183 (2010) 1216–1230, http://dx.doi.org/10.1111/j.1365-246X.2010.04804.x.
[35] J.R. Wertz (Ed.), Spacecraft Attitude Determination and Control, Kluwer Academic Publishers, 1978. ISBN: 978-9027712042.